Chemical study of fly ash deposition in combustion of pelletized residual agricultural biomass

Javier Royo; Paula Canalís; David Quintana;

University of Zaragoza, c/ María de Luna 3, E-50018 Zaragoza, Spain

ABSTRACT

Agricultural residual biomass has great potential as an energy source, but is used only to a limited extent mainly because of the characteristics of its ash (quantity and composition), which can lead to problematic phenomena during combustion, among them fly ash deposition, the focus of this study. A previous work presented the results of laboratory experiments carried out using a fixed-grate reactor and involving four different agropellets under different operating conditions; the variables tested were deposition rate, bottom ash proportion and sintering degree during combustion. Based on these results, the analysis has been taken further and the fly ash deposits collected during these tests have been characterized by SEM-EDS and XRD. A methodology to differentiate between deposits caused by condensation (including thermophoresis and turbulent diffusion) and by inertial impact of coarse fly ash entrained from the bed has been proposed. Deposition by condensation has been found to decrease for higher values of excess air ratio in all cases. Conversely, deposition by inertial impact does not show a common behavior, due to the influence of bottom ash sintering degree and fuel composition. The ultimate aim of this study is to gain a better understanding of fly ash deposition, in order to develop better fuel blends, boiler design and operating parameters, enhancing the market penetration of agricultural residual biomass.

KEY WORDS:

Agricultural residual biomass; Combustion; Fixed bed reactor; Fly ash deposition; SEM-EDS; XRD

1. INTRODUCTION

The main contribution of biomass to the generation of renewable energy in the EU is found in the heating and cooling sector [1], where important growth is expected in coming years; the target for 2020 having been set at 3785 PJ [1]. New uses for forest biomass ([2], [3]), in addition to the traditional energy production, make imperative to find new resources with which to meet the predictable rise in demand for thermal energy. The biggest growth in supply should come from the agricultural sector, where an increase of over 150% compared with 2006 is expected [1].

In addition to energy crops and some types of residual agro-industrial biomass, these new resources mainly comprise agricultural crop residues: herbaceous crop residues and pruning residues of permanent woody crops. In particular, this paper focuses on three residual agricultural biomasses: vineyard pruning residues, corn stover and barley straw. These were selected due to their potential as sources of energy both in Europe and the rest of the world. FAOSTAT data (available at [4]) indicate that the area covered by vines and maize and barley crops in the EU in 2017 was nearly 23.4 Mha. Using conservative availability indices (50% for vineyard pruning residue and corn stover, and 10% for barley straw), this translates into an energy potential of over 500 PJ/yr for the EU. In consequence, their use could contribute significantly to achieve the objectives set.

Thermal conversion of agricultural biomass, mainly of the herbaceous type, shows clear differences compared with forest biomass. This is mainly due to the characteristics of the ash (quantity and composition), which can lead to certain problems in conversion facilities.

During combustion, ash undergoes physical and chemical transformations which cause fractioning. Part of the components of the ash remain as a solid fraction which accumulates in the grate (bottom ash) and in some cases can sinter, affecting conversion in the bed, restricting efficiency of the grate and negatively affecting the control of gaseous emissions: carbon monoxide, nitrogen oxides, and volatile organic compounds ([5]-[9]).

Other part, mainly related with alkali metal compounds, is volatilized. After complex and not always well known mechanisms ([10], [11]), these compounds can directly condense or after forming

aerosols be deposited by thermophoresis and/or turbulent diffusion ([11]-[13]) on the surfaces of the equipment used for heat exchange, in the form of small crystals (e.g., potassium chloride -KCl-, potassium sulfate -K_2SO_4- and potassium carbonates -K_2CO_3 and $KHCO_3$-). An ash entrainment of solid particles (coarse fly ash) in gas combustion flow from the bed can also be generated and, in some conditions, these particles can be deposited on convective areas by inertial impact. These phenomena (volatilization and ash entrainment) are responsible, alongside deposition, for corrosion and erosion, which reduce equipment performance and use-life ([5], [9]).

In recent decades, several prestigious research centers have been working towards identifying key factors in the conversion of biofuels, as well as in the transformation of their ash, in order to understand problems caused by the latter ([8], [14]-[23]). In all cases, the critical influence of ash chemical composition, especially the concentration of Na, Mg, Al, Si, P, S, Cl, K and Ca [24], is recognized in issues associated with thermal conversion (e.g. sintering, deposition, corrosion, erosion and emissions). However, chemical composition is not the only factor, since ash behavior is also affected by combustion conditions in the bed, which are themselves related to design ([23]-[26]) and operational parameters [27].

Owing to the complexity of the phenomena that contribute to ash fractioning, combustion tests are often undertaken in laboratory reactors, most of which operate with a fixed-grate in order to keep combustion conditions under control ([23],[28]-[32]). This type of reactor enables, in the simplest way, the collection of important information concerning the behavior of fuels under different operating conditions. It allows the evaluation of fuel reactivity (ignition front velocity and ignition rate [33]), quantifying of bottom ash in the bed and determining its propensity to sintering, as well as quantifying the amount of solid residue deposited on heat exchange surfaces per time and unit area (deposition rate) [31]. Furthermore, these reactors allow samples to be taken for the characterization of solid residues (bottom ash fraction and fly ash deposits), allowing a better understanding of the phenomena driving ash fractioning. In addition, the analysis of gaseous (e.g. CO, NOx or volatile organic compounds) ([34]-[37]) and particle emissions ([38]-[40]), is also possible.

In a previous work [41], authors presented the results analysis of the four first points (reactivity, bottom ash quantity, sintering degree and deposition rate) for different pellets made of residual agricultural biomass (agropellets). These pellets were evaluated under a range of operating conditions in a laboratory fixed-grate reactor. In this paper, it is intended to go a step further and characterize fly ash deposition samples collected in combustion tests by means of scanning electron microscopy (SEM) with energy dispersive X-ray spectrometry (EDS), and powder X-ray diffractometry (XRD). These methods are widely used to identify and characterize ash compounds ([9],[13], [42]-[48]).

SEM-EDS provides detailed imaging information about morphology, as well as defining the elemental chemical composition of samples. This technique is both easy and highly precise. Although elements which are present in concentrations below 0.1-0.5% are below detection limits [42], in general it does not affect the detection of the previously commented most significant ash-forming elements responsible for ash-related operational problems during combustion.

The XRD method is applied to identify and quantify crystalline phases present in the sample by measuring their concentrations, as well as determining the amorphous fraction [42].

These are complementary techniques. On the one hand, XRD allows for a better understanding of how chemical elements detected by SEM-EDS are associated. On the other hand, the identification of minor minerals in a multicomponent system by means of XRD is uncertain due to such issues as detection limits, peak overlapping and unknown amorphous matter. SEM-EDS results facilitate the identification of phases and can provide confirmation of XRD results [49].

From the results obtained by means of SEM-EDS and XRD, a methodology is proposed to differentiate between deposits caused by condensation (including thermophoresis and turbulent diffusion) and by inertial impact of coarse fly ash entrained from the bed.

The ultimate aim is to gain a better understanding of deposition phenomena affecting agricultural residual biomass. This will, it is hoped, help researchers and technologists to make better decisions

regarding fuel blends, boilers design and optimum operating parameters, increasing the market penetration of this important type of biomass.

2. MATERIAL AND METHODS

2.1 Fuels

Fly ash deposition chemistry of four different agropellets (agricultural residual pellets) is studied in this paper:

- Woody agropellet: 100% Vineyard pruning pellet (PV)[1]
- Mixed agropellets (Vineyard pruning blended with an herbaceous component):
  - 70% Vineyard pruning + 30% Barley straw (PVB)
  - 70% Vineyard pruning + 30% Corn stover (PVC)
  - 60% Vineyard pruning + 20% Corn stover + 20% Barley straw (PVCB).

The main thermochemical properties of selected fuels are reproduced from [41] and shown in Tables 1 and 2.

Table 1
Fuel properties (% m/m: mass percentage; d.b.: dry basis; w.b.: wet basis).

		PV	PVB	PVC	PVCB
Bulk density (kg·m^{-3})[a]		599	562	556	546
Proximate analysis (% m/m d.b.)	Volatile matter[b]	76.5	72.4	72.1	72.3
	Fixed carbon[c]	20.5	21.7	18.6	21.2
	Ash[d]	3.1	5.9	9.3	6.5
Total moisture (% m/m w.b.)[e]		9.0	9.1	9.2	9.0
Ultimate analysis (% m/m d.b.)	Carbon[f]	48.9	46.36	46.01	46.36
	Hydrogen [f]	5.8	5.77	5.64	5.55
	Nitrogen [f]	0.55	0.56	0.55	0.60
	Sulfur [g]	0.09	0.055	0.050	0.094
	Chlorine [g]	0.03	0.047	0.080	0.090
	Oxygen [c]	41.6	41.29	38.33	40.58
HHV (d.b. at p=constant) (MJ·kg^{-1})[h]		19.11	18.54	18.06	18.36
LHV (w.b. at p=constant) (MJ·kg^{-1})[h]		16.01	15.48	15.06	15.40

[a] EN 15103:2009 [b] EN-ISO 18123:2016 [c] Calculated [d] EN-ISO 18122:2016 [e] EN-ISO 18134:2016
[f] EN-ISO 16948:2015 [g] EN-ISO 16994:2015 [h] EN-ISO 14918:2011

[1] Vineyard pruning residues used to produce this agropellet were not the same as those used for mixed agropellets.

Table 2
Ash properties (% m/m: mass percentage; d.b.: dry basis).

		PV	PVB	PVC	PVCB
Chemical ash composition (% m/m d.b.)[a]	Al_2O_3	0.91	2.72	2.19	2.30
	CaO	42.39	45.77	48.17	40.54
	Fe_2O_3	0.71	2.22	1.98	1.27
	K_2O	30.09	14.88	15.79	19.43
	MgO	10.45	8.64	7.64	11.01
	Na_2O	0.62	0.41	0.39	0.38
	P_2O_5	7.35	4.45	4.00	4.36
	SO_3	3.95	2.32	3.24	4.39
	SiO_2	2.65	17.70	15.31	15.22
	TiO_2	0.07	0.17	0.18	0.16
	Cl	0.12	0.21	0.57	0.54
Ash melting points in oxidizing conditions (°C)[b]	Initial deformation temperature (DT)	1240	1130	1310	1330
	Hemisphere temperature (HT)	> 1500	1310	1460	1460
	Flow temperature (FT)	> 1500	1370	1480	1470

[a] EN-ISO 16967:2015 [b] CEN/TS 15370-1:2006

2.2 Reactor

As noted, research of ash-related phenomena during combustion is generally carried out with the aid of laboratory reactors. In the case of fixed-bed reactors, simplified geometries are used to being able to consider one-dimensional behavior [50].

In order to perform the combustion tests, an experimental fixed-grate reactor was used (see Fig. 1). In this reactor, inlet air is injected through the grate from the bottom by means of a fan equipped with a variable-frequency drive which allows airflow to be regulated. Since experiments require inlet air temperature to remain under control, the reactor is equipped with a refrigerator and an electrical resistor either to cool the air or heat it as needed. This allowed two different types of tests to be undertaken: without preheating (inlet air at 25°C) and with preheating (inlet air at 80°C). The reactor is fitted with fifteen N thermocouples to monitor temperature both at the bed and the freeboard.

In addition, the facility includes a deposition probe, with a removable sampling ring in the chimney of the reactor [51]. This is a common device used to simulate fly ash deposition in furnace pipes and heat exchangers [49]. Prior to the experiment, the removable sampling ring is cleaned, dried,

measured and weighed. During the stable combustion period, the deposition probe is inserted inside the chimney and the ring is cooled by compressed air, keeping its surface at an appropriate temperature for studying deposition [51]. For the tests presented here, compressed inlet air was adjusted to keep an average temperature of 335±25ºC. Once extracted, the dirty ring is dried and weighed again to determine the mass of deposits, allowing deposition rate (DR, $g \cdot m^{-2} \cdot h^{-1}$) to be calculated and, thus, the different propensity of each fuel used for deposition to be assessed ([31], [41], [52]-[56]).

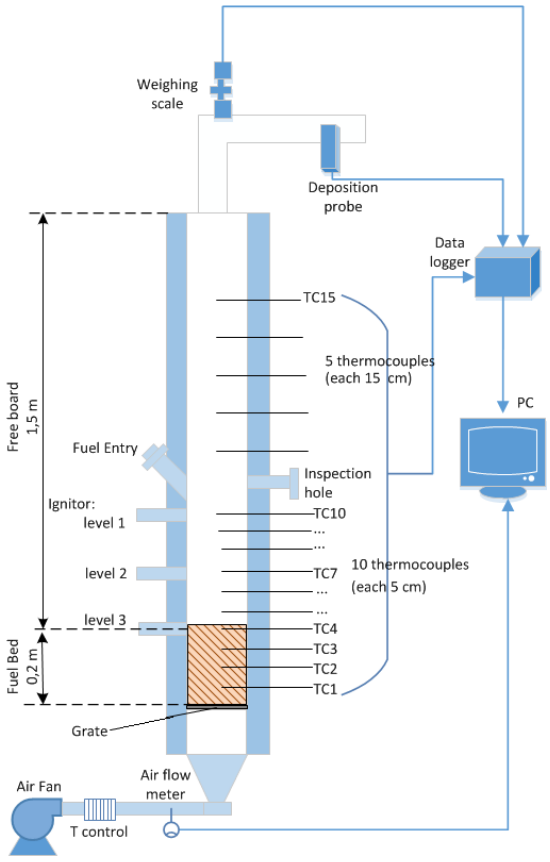

Fig. 1. Scheme of the experimental test facility [41].

Finally, once combustion is completed and the reactor cools down, bottom ash is collected from the surface of the grate for weighing and classification, which allows the sintering tendency of each fuel to be determined ([5], [21], [41], [57], [58]). Three fractions were considered: S1, which passes through a 3.15 mm sieve and is considered to be not sintered; S2, which does not pass through a 3.15 mm sieve, but is easily disaggregated by hand and presents a low sintering degree; S3, which does not pass the

3.15 mm sieve, is difficult to disaggregate by hand and presents a high sintering degree. Since the difference between S2 and S3 is subjective, a fraction S2/3 encompassing both classes was used.

2.3 Ash analysis

In all the tests, once deposits had been weighed and deposition rate calculated, a sample was taken from the front face of the removable sampling rings, that is, from the side facing and perpendicular to the flow of combustion gases. Samples of S1 bottom ash fractions were also collected. All samples were glued onto metal plates with carbon tape and coated with carbon before being analyzed by SEM-EDS. The equipment used was a Carl Zeiss Merlin electronic field emission microscope equipped with Gemini Column, with acceleration voltages between 0.02 and 30 kV, fitted with an EDS X-MAS detector by Oxford Instruments with a window of 20 mm^2 and energy resolution between 127 eV and 5.9 keV. For each sample, three 1 mm^2-zones were selected, and images taken with the retro-dispersed detector (asb). Average elemental composition was obtained through EDS, using a voltage of 15 kV. INCA software was used to process the results. Major participating elements in the most important ash transformation processes -namely Na, Mg, Al, Si, P, S, Cl, K, Ca and Fe- were included in the analysis.

In addition, four combustion experiments without air preheating were selected for each fuel. These tests were chosen to cover evenly the common range of excess air ratio (λ) for each fuel (see Table 3). A preheated experiment was also selected for each agropellet, all four with an almost identical excess air ratio value ($\lambda \approx 1.3$). For all these tests the crystalline matter composition of the fly ash deposition samples collected in the ring was determined by XRD. Standard X-ray diffraction patterns were collected at room temperature using a Rigaku D/max instrument with a copper rotating anode and a graphite monochromator to select CuKα wavelength. The measurements were performed at 40 kV and 80 mA, in the angular range from 5° to 80° on 2θ, applying a step size of 0.03° and a counting rate of 1 s/step. X-ray patterns were analyzed with JADE software, with access to the JCPDS-International Centre for Diffraction Database (2000) and profile-based RIR analyses.

3. RESULTS AND ANALYSIS

3.1. Tests and results

A total of 68 combustion tests were carried out following the same protocol with the four fuels. As already noted tests both with and without preheating ("ph" experiments) – varying inlet air temperature (Ta) – were undertaken for every fuel. In the tests the excess air ratio ranged from 1.1 to 2.3 (over-stoichiometric conditions), in order to reproduce the combustion conditions found in small domestic equipment. Table 3 summarizes the main features of the experiments performed.

Table 3
Outline of test features.

		PV	PVB	PVC	PVCB
Number of tests performed	**Without preheating (Ta=25 °C)**	10	10	10	12
	Preheated tests (-ph-; Ta=80 °C)	8	6	6	6
λ	**Min**	1.15	1.21	1.18	1.23
	Max	2.04	2.30	2.29	2.07
Fed fuel (kg)		4.03	3.78	3.74	3.67

Table 4 shows mean values (and range) of elemental composition obtained by SEM-EDS for each of the four fuels of fly ash deposits, expressed as a percentage of the total mass of measured elements (Na, Mg, Al, Si, P, S, Cl, K, Ca and Fe).

Furthermore, Fig. 2 plots the values summarized in Table 4 against excess air ratio, keeping out the elements with a concentration significantly lower than 10 % in all the samples (Al, Si, P and Fe) of fly ash deposits collected in the combustion experiments (with and without preheating). Due to their chemical similarity and the almost identical role they play in the reactions that take place in ash transformation processes, the concentrations of K and Na [24] as well as Ca and Mg [59] have been aggregated in Fig. 2.

Table 4

Mean values (range) of the elemental composition (SEM-EDS) of fly ash deposits expressed as a percentage of the total mass of measured elements (Na, Mg, Al, Si, P, S, Cl, K Ca and Fe). Test without and with (ph) inlet air preheating (% m/m: mass percentage).

FUEL	SEM-EDS analysis results (%m/m)									
	Na	**Mg**	**Al**	**Si**	**P**	**S**	**Cl**	**K**	**Ca**	**Fe**
PV	0.48 (0.35-0.67)	4.80 (3.40-7.33)	0.25 (0.15-0.35)	0.64 (0.40-0.86)	3.50 (2.40-5.30)	6.91 (5.38-8.66)	5.54 (3.04-9.35)	49.84 (40.26-57.93)	27.66 (21.03-36.61)	0.39 (0.23-0.52)
PV (ph)	0.41 (0.24-0.51)	6.09 (4.20-7.67)	0.37 (0.21-0.70)	0.74 (0.59-0.91)	4.32 (3.12-5.14)	5.68 (4.96-6.48)	6.29 (3.71-10.68)	40.87 (34.46-47.30)	34.77 (27.97-42.06)	0.46 (0.29-0.64)
PVB	0.28 (0.20-0.38)	0.72 (0.36-1.07)	0.27 (0.11-0.37)	1.21 (0.57-1.81)	0.51 (0.25-0.69)	8.21 (6.91-10.03)	24.20 (20.56-27.41)	57.99 (53.27-62.07)	6.34 (3.31-8.92)	0.27 (0.07-0.48)
PVB (ph)	0.28 (0.20-0.41)	0.98 (0.35-1.54)	0.32 (0.17-0.45)	1.35 (0.50-2.27)	0.70 (0.29-1.11)	7.21 (6.09-8.68)	24.39 (21.46-28.31)	56.77 (53.41-60.30)	7.67 (2.59-11.93)	0.34 (0.10-0.56)
PVC	0.25 (0.19-0.30)	2.60 (1.18-4.28)	0.66 (0.35-1.08)	3.12 (1.39-4.54)	1.36 (0.74-2.41)	6.07 (5.17-8.10)	20.77 (14.23-27.57)	40.09 (28.42-49.57)	24.46 (11.88-38.82)	0.62 (0.27-1.13)
PVC (ph)	0.23 (0.20-0.25)	3.33 (2.14-4.03)	0.76 (0.51-0.98)	3.38 (2.10-3.97)	1.73 (1.22-2.30)	5.33 (4.63-6.25)	17.57 (14.62-22.50)	37.64 (33.74-46.29)	29.38 (18.41-34.15)	0.65 (0.35-0.86)
PVCB	0.26 (0.16-0.35)	2.89 (1.56-4.94)	0.75 (0.45-1.28)	3.55 (2.26-5.31)	1.61 (0.88-2.71)	7.80 (5.94-10.12)	16.41 (9.20-20.19)	44.37 (32.91-53.16)	21.63 (13.04-35.71)	0.72 (0.48-1.18)
PVCB (ph)	0.28 (0.24-0.33)	3.54 (1.81-4.32)	0.83 (0.48-1.07)	3.78 (1.87-5.08)	2.11 (1.28-2.66)	6.79 (5.61-7.65)	14.11 (12.00-20.15)	42.28 (37.13-52.14)	25.58 13.93-31.32)	0.70 (0.44-0.90)

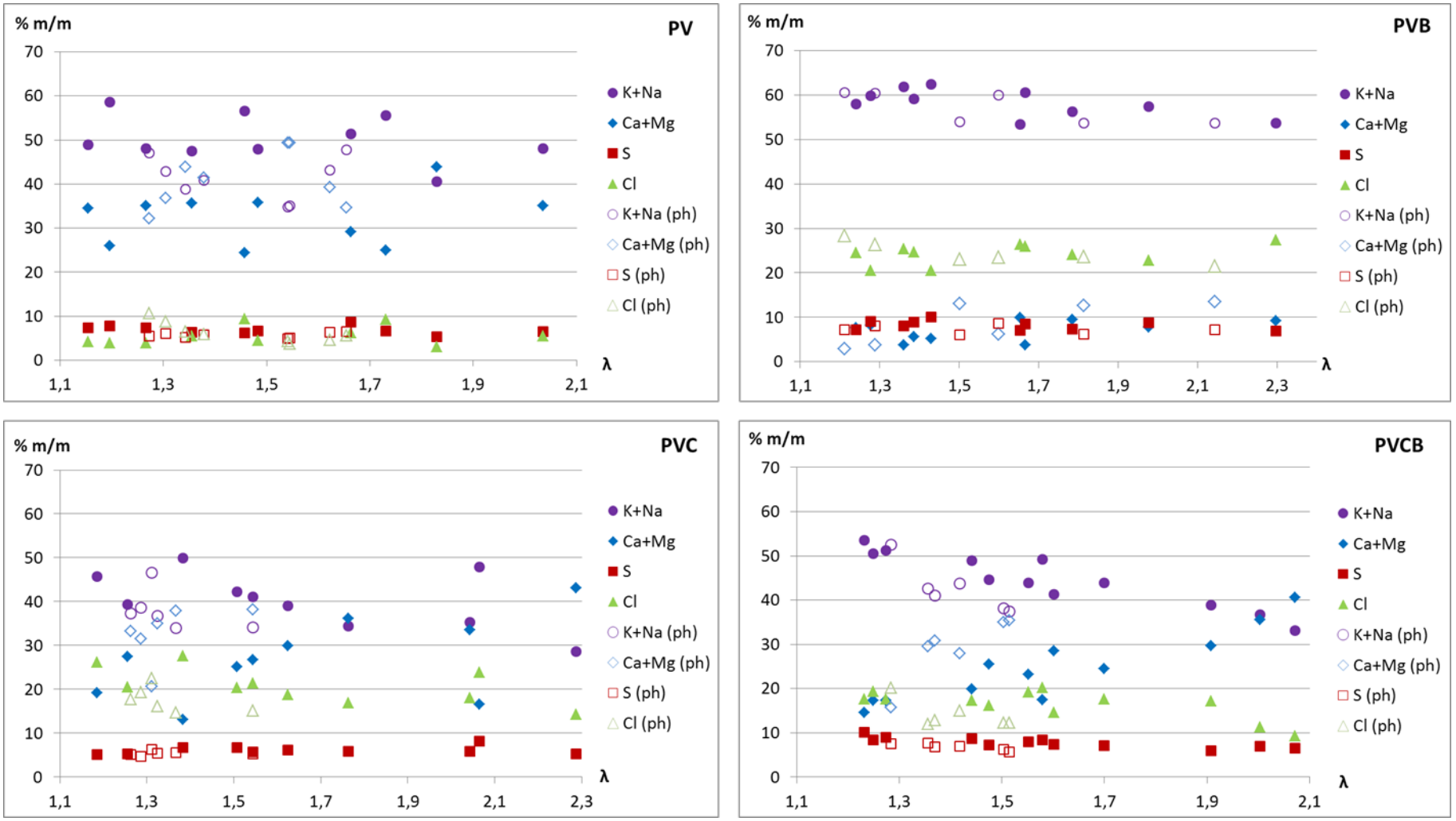

Fig. 2. Elemental composition (SEM-EDS) of fly ash deposits expressed as a percentage of the total mass of measured elements (Na, Mg, Al, Si, P, S, Cl, K, Ca and Fe) against excess air ratio (λ) for PV, PVB, PVC and PVCB (% m/m: mass percentage).

Table 5 shows the crystalline phases and amorphous concentrations detected in the samples of five selected tests per fuel using XRD.

Although a preliminary analysis can be made from data presented in Fig. 2 and Table 4 and 5, in subsection 3.3 an analysis methodology is proposed to expand the study of these results. In order to apply this methodology, it was also necessary to determine the elemental composition of S1 bottom ash fractions by SEM-EDS. Results are shown in Fig. 3 (only Na, Si and K) as a function of excess air ratio (with and without preheating tests).

Table 5

Deposits composition (selected combustion tests).

FUEL	λ	XRD analysis results								
		Crystalline matter (%)[a]								Amorphous[b] (%)[c]
		KCl	K_2SO_4	$KHCO_3$	$CaCO_3$	SiO_2	Ca_2SiO_4	MgO	$Ca(OH)_2$	
PV	1.16	1.6	19.6	15.5	21.9			31	10.3	-[d]
	1.46	5.5	19.6	21.2	18.4			25	10.3	-[d]
	1.73	7.9	19.8	36.7	11.9			19.4	4.3	-[d]
	2.04	4.8	21.8	27.6	17.1			21.2	7.4	-[d]
	Mean	**5.0**	**20.2**	**25.3**	**17.3**	**0**	**0**	**24.1**	**8.1**	-[d]
	1.34 (ph)	3.2	15.2		61.0			20.6		25.5
PVB	1.24	29.6	34.5		23.8	4.2	7.8			12.1
	1.67	42.1	25.3	18.0	10.3	4.2				6.7
	1.98	36.9	29.4		33.7					20.1
	2.30	41.1	31.3		27.6					14.2
	Mean	**37.4**	**30.1**	**4.5**	**23.9**	**2.1**	**2.0**	**0**	**0**	**13.3**
	1.29 (ph)	34.4	29.1		31.4	5.1				24.0
PVC	1.18	30.0	18.4		35.7	6.1	6.5		3.3	17.4
	1.38	27.7	23.7		33.9	3.8	6.8		4.2	12.9
	1.76	27	23.7		32.7	6.6	6.2		3.7	5.4
	2.29	13.3	14.3		55.6	2.2	8.6		6	18.7
	Mean	**24.5**	**20.0**	**0**	**39.5**	**4.7**	**7.0**	**0**	**4.3**	**13.6**
	1.31 (ph)	32.6	18.8		41.3	7.4				21.4
PVCB	1.23	27.1	41.9		26.5	4.5				16.6
	1.44	24.2	38.3		25.9	11.6				18.9
	1.70	27.8	34.3		33.7	4.2				13.8
	2.07	15.9	29		45.3	9.8				9.2
	Mean	**23.8**	**35.9**	**0**	**32.9**	**7.5**	**0**	**0**	**0**	**14.6**
	1.28 (ph)	26.1	34.0		31.2	8.8				19.3

[a] Expressed as mass percentages with regard to the total amount of crystalline matter in the deposits.

[b] A conservative approach to amorphous matter was adopted, and only crystallite size (XS) under 80 Å was included (crystalline matter with low particle size can be included).

[c] Expressed as mass percentage with regard to the total amount of deposit.

[d] Cannot be determined because small size of samples leads to too much noise in the diffractogram.

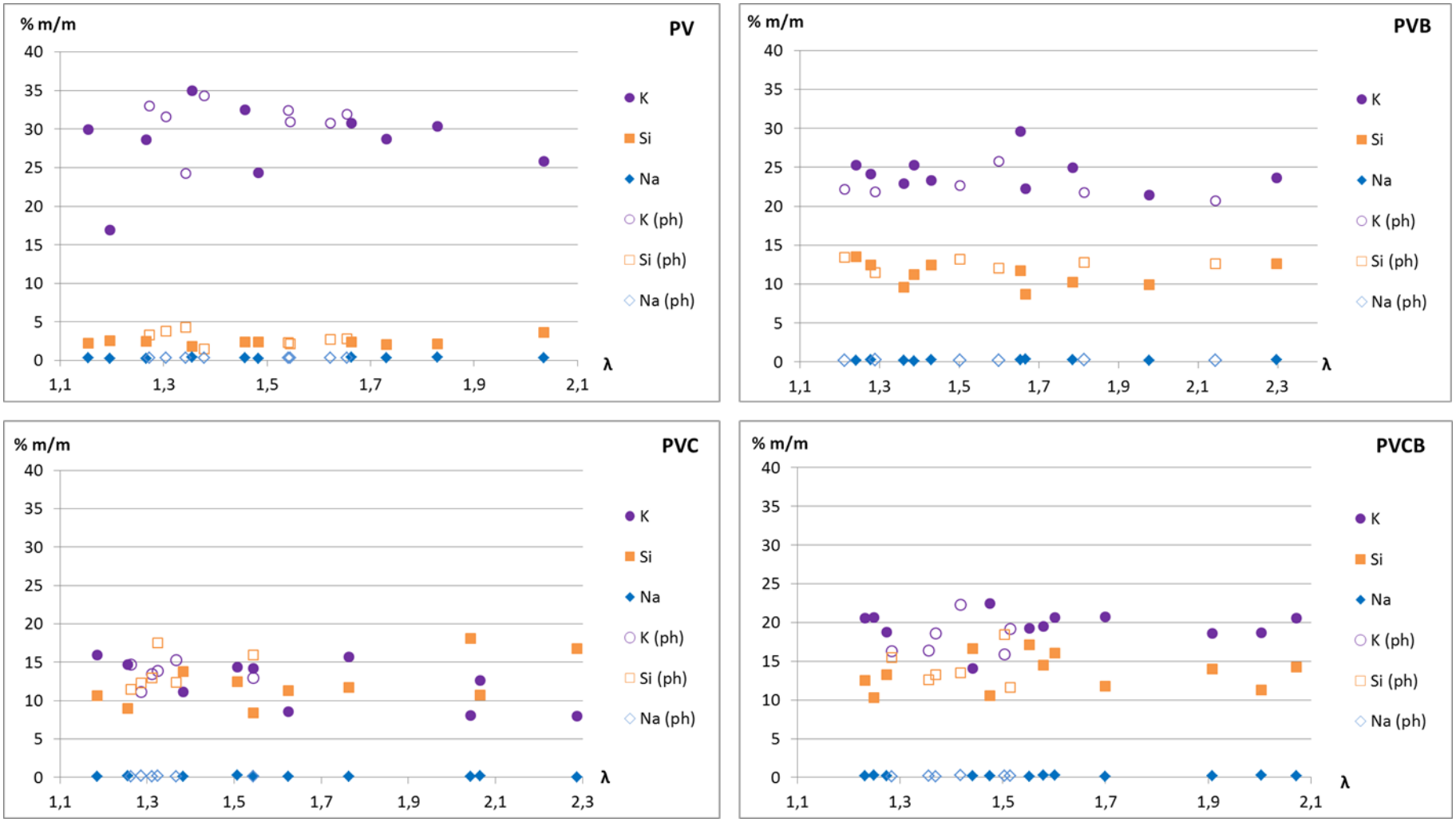

Fig. 3. Elemental composition (SEM-EDS) of S1 bottom ash fraction expressed as a percentage of the total mass of measured elements (Na, Mg, Al, Si, P, S, Cl, K, Ca and Fe) against excess air ratio (λ) for PV, PVB, PVC and PVCB (% m/m: mass percentage).

3.2. Preliminary analysis

Based on the results presented in Figure 2 and Tables 4 and 5 of the previous subsection, an initial analysis can be made regarding deposition phenomena for the various fuels.

In Fig. 2 it can be noted that in all cases, the main elements present in the ash deposited in the sampling ring are K+Na, the percentage of which tends to decrease as excess air ratio increases (especially in the case of PVCB). Also noteworthy is the high concentration of Ca+Mg, except in the case of PVB. In contrast to K+Na, concentration of alkaline earth metals increases with greater excess air ratios, especially in the case of PVCB. Concentration of Cl is also significant, except for PV. S content does not vary significantly for all the fuels and along the whole excess air ratio range analyzed, remaining slightly below 10 %. The remaining elements measured (Al, Si, P and Fe) present concentrations below 6% in all cases (see Table 4).

In line with SEM results, XRD findings (Table 5) underline the high concentration of alkali metal compounds, mainly KCl -although this is not the case with PV, also endorsed by SEM results- and K_2SO_4, but also $KHCO_3$ in the PV case and in a sample of PVB. Compounds of Ca ($CaCO_3$, Ca_2SiO_4 and $Ca(OH)_2$) and to a lesser extent of Si (SiO_2) are very abundant too, except in PV, in which the latter compound does not appear because of its low Si content, MgO taking its place. Based on XRD results, it is not possible to determine clear tendencies between excess air ratio and compounds concentration, which remain fairly constant across the analyzed range.

Concerning the effect of inlet air temperature, Fig. 2 illustrates the increase in concentration of Ca+Mg for all fuels, and the slight decrease in K+Na (except for PVB) and Cl (except for PV and PVB) in tests involving preheating. The decrease in K+Na is especially remarkable in the case of PV, as is also indicated by XRD results, because the concentration of K compounds in preheated tests is significantly lower (even $KHCO_3$ does not appear).

With regard to the amorphous matter fraction, Table 5 shows lower values for tests without preheating (13.9 % on average) than with preheating (21.6 % on average).

245 The differences in the behavior of each fuel observed in Fig. 2 and Table 5, concerning both deposits
246 composition and trends related to excess air ratio and inlet air temperature, are probably related to
247 the importance of the various deposition mechanisms that apply for each fuel, and of the operating
248 conditions.

249 ### 3.3. Deposition mechanisms analysis

250 This subsection aims to go in depth in the analysis of fly ash deposition phenomena for the four fuels
251 under consideration in relation to ash composition, excess air ratio and inlet air temperature.
252 As noted in [41], the increase in excess air ratio leads to less ash deposition in the probe for all
253 agropellets. In order to analyze this result in detail and to enable practical conclusions to be reached,
254 deposition process will be divided into two mechanisms.
255 There are two ways in which ash can leave the bed, by vaporization and by entraining. Each of these
256 leads to a different deposition mechanism, one produced by condensation and another by inertial
257 impact, respectively:

258 - Condensation: some compounds, mainly alkali-metal chlorides, sulfates and hydroxides,
259 are vaporized and can be deposited on the heating surface chiefly as chlorides, sulfates
260 and carbonates by direct condensation or after forming aerosols by thermophoresis or
261 turbulent diffusion. In the case of alkali metal sulfates and chlorides, because of their low
262 melting points, a sticky layer is formed, to which other deposits adhere ([11], [12], [52],
263 [60]-[62]). Part of these alkali metal compounds can also condense into coarse fly ash
264 ([11], [12], [60]-[63]).
265 - Inertial impact: some of the coarse fly ash entrained from the bed, which contained
266 mainly silicates, aluminosilicates and phosphates, as well as oxides, carbonates, sulfates,
267 and hydroxides of Mg, Si, Ca and/or Fe, can form deposits on the sticky initial layer by
268 inertial impact ([11], [12], [52], [60]-[62]).

The alternate combination of deposits by condensation and by inertial impact results in the construction of an overlapping multi-layered structure ([12], [60]).

In the following subsection, it is proposed a methodology that allows estimating the percentage and the amount of ash deposited by each of these two processes.

3.3.1. Methodology description

The two mechanisms involved in ash deposition are highly complex, and it is helpful to stablish several simplifications in order to facilitate the analysis of results.

A first set of assumptions is related to bottom ash and the entrainment of coarse fly ash. It is assumed that Si forms compounds (silicates, aluminosilicates and oxides) that remain solid regardless of combustion temperatures ([12], [24]). Consequently, all Si present in the sampling ring (subscript "Probe") is assumed to have been deposited by inertial impact (subscript "Imp.")[2]:

$$Si_{Probe} = Si_{Imp.} \quad (1)$$

It has been reported that the chemical composition of coarse fly ash entrained from the bed resembles that of bottom ash ([52], [64]). For the development of this methodology it is only necessary to consider that Si/K proportion in S1 fraction (subscript "S1", a fraction that is constituted by particles that can be easily dragged) remains the same in entrained ash (which can subsequently be deposited by inertial impact). This assumption, together with equation (1), leads to the following equation (2):

$$(K/Si)_{S1} = (K/Si)_{Imp.} = K_{Imp.} / Si_{Probe} \quad (2)$$

Following equation (2), and considering that, out of the total amount of K found in sampling ring deposits, a fraction can be ascribed to inertial impact of solids entrained directly from the bed, with the remainder ascribed to condensation (subscript "Cond."), equation (3) follows:

$$K_{Cond.} = K_{Probe} - K_{Imp.} = K_{Probe} - (K/Si)_{S1} \cdot (Si)_{Probe} \quad (3)$$

The argumentation that leads to equations (2) and (3) would also work for Na instead of K.

[2] In equations (1) to (3) "Si" and "K" can be mass or molar contents of each element.

293 A second set of considerations is related to the compounds present in deposits. Based on XRD results
294 (see Table 5), crystalline phases related chlorides, sulfates and carbonates of alkali metals
295 (condensation) are KCl, K_2SO_4, $KHCO_3$, while those related to Mg, Si and Ca (inertial impact) are
296 $CaCO_3$, $Ca(OH)_2$, MgO, SiO_2 and Ca_2SiO_4.
297 Bearing in mind the molecular mass of the aforementioned compounds, it can be noted that:
298 • 1 kg of $K_{Cond.}$ present in the probe implies 1.9 kg of KCl, 2.23 kg of K_2SO_4 or 2.56 kg of
299 $KHCO_3$. That is to say, 1 kg of $K_{Cond.}$ implies deposits of the order of 2 kg forming KCl,
300 K_2SO_4 and/or $KHCO_3$. Other chlorides, sulfates and carbonates of alkali metals which can
301 be volatilized and then deposited by condensation, even those which do not appear in
302 these XRD results (e.g. K_2CO_3 and $K_3Na(SO_4)_2$), also follow, in order of magnitude, the
303 proportion of 2 kg of deposits per kg of K+Na[3].
304 • 1 kg of Ca present in the probe implies 1.85 kg of $Ca(OH)_2$ or 2.5 kg of $CaCO_3$; 1 kg of Mg
305 implies 1.67 kg of MgO; 1 kg of Si implies 2.14 kg of SiO_2; 1 kg of Ca+Si (0.74 kg of Ca +
306 0.26 kg of Si) implies 1.59 kg of Ca_2SiO_4. That is to say, 1 kg of Ca+Mg+Si also implies
307 deposits of the order of 2 kg in the form of MgO, $CaCO_3$, $Ca(OH)_2$, SiO_2 and/or Ca_2SiO_4.
308 Likewise, the compounds of Ca, Mg, Si, P, Al and/or Fe, which are typically formed in
309 combustion and can be entrained from the bed (mainly silicates, aluminosilicates,
310 phosphates, oxides, carbonates, sulfates, and hydroxides, where K and Na can also be
311 present [65]), also follow, in order of magnitude, the proportion of 2 kg of deposits per
312 kg of Ca+Mg+Si+P+Al+Fe+K+Na[4].
313 In view of the fact that, on one side, each mass unit of $K_{Cond.}$+$Na_{Cond.}$ and, on the other side, of
314 Ca+Mg+Si+P+Al+Fe+ $K_{Imp.}$+$Na_{Imp.}$ produces approximately (in terms of order of magnitude) the same
315 amount of deposits, it is possible to approximately determine the mass ratio of deposits due to

[3] If the 7 compounds of this type mentioned in [65] with a presence over 1 % are considered, it is obtained a maximum value of 2.52, minimum of 1.77 and mean (unweighted) of 2.19 kg of deposits per each kg of K+Na (deposited by condensation).

[4] If the 45 compounds of this type mentioned in [65] with a presence over 1 % are considered, it is obtained a maximum value of 3.40, minimum of 1.40 and mean (unweighted) of 1.93 kg of deposits per each kg of Ca+Mg+Si+P+Al+Fe+K+Na (for alkalis, the fraction from deposits by inertial impact is only included).

316 condensation ($DM_{Cond.}$, kg) and inertial impact (DM_{Imp}, kg) according to equation (4)[5]:

317 $$DM_{Cond.}/DM_{Imp.} = (K+Na)_{Cond.}/((Ca+Mg+Si+P+Al+Fe)_{Probe} + (K+Na)_{Imp.}) \quad (4)$$

318 Taking into account the relationship shown in equation (4), the mass fraction of deposits caused by
319 condensation ($mf\_deposits_{Cond.}$) and inertial impact ($mf\_deposits_{Imp.}$) can be accounted for, as shown
320 in equations (5) and (6):

321 $$mf\_deposits_{Cond.} = DM_{Cond.}/(DM_{Cond.} + DM_{Imp.}) =$$

322 $$= (K+Na)_{Cond.}/((K+Na)_{Cond.} + ((Ca+Mg+Si+P+Al+Fe)_{Probe} + (K+Na)_{Imp.})) =$$

323 $$= (K+Na)_{Cond.}/(K+Na+Ca+Mg+Si+P+Al+Fe)_{Probe} \quad (5)$$

324

325 $$mf\_deposits_{Imp.} = DM_{Imp.}/(DM_{Cond.} + DM_{Imp.}) =$$

326 $$= ((Ca+Mg+Si+P+Al+Fe)_{Probe} + (K+Na)_{Imp.})/((K+Na)_{Cond.} + ((Ca+Mg+Si+P+Al+Fe)_{Probe} + (K+Na)_{Imp.})) =$$

327 $$= ((Ca+Mg+Si+P+Al+Fe)_{Probe} + (K+Na)_{Imp.})/(K+Na+Ca+Mg+Si+P+Al+Fe)_{Probe} \quad (6)$$

328 By multiplying each of these mass fractions by the deposition rate it is possible to share out the total
329 mass of deposits between both mechanisms, obtaining the deposition rate by condensation ($DR_{Cond.}$,
330 $g \cdot m^{-2} \cdot h^{-1}$) and by inertial impact ($DR_{Imp.}$, $g \cdot m^{-2} \cdot h^{-1}$), equations (7) and (8):

331 $$DR_{Cond.} = mf\_deposits_{Cond.} \cdot DR \quad (7)$$

332 $$DR_{Imp.} = mf\_deposits_{Imp.} \cdot DR \quad (8)$$

333 Naturally, this methodology only provides approximate values, but based on some reasonable
334 hypotheses and simplifications, it allows obtaining conclusions about the mechanisms of deposition
335 (condensation or inertial impact), as can be seen in next subsection.

336 ### 3.3.2. Methodology application and discussion

337 The combination of the elemental composition (SEM-EDS) of ring deposits (Fig. 2 and Table 4) and S1
338 bottom ash fractions (Fig. 3), the deposition rate [41] and equations (3) to (8), leads to Fig. 4, which
339 expresses deposition rates by condensation and by inertial impact as a function of excess air ratio for
340 each of the four fuels analyzed (tests with and without preheating are shown).

[5] In equations (4) to (6) "Ca", "Mg", "Si", "P", "Al", "Fe", "K" and "Na", are mass contents of each element.

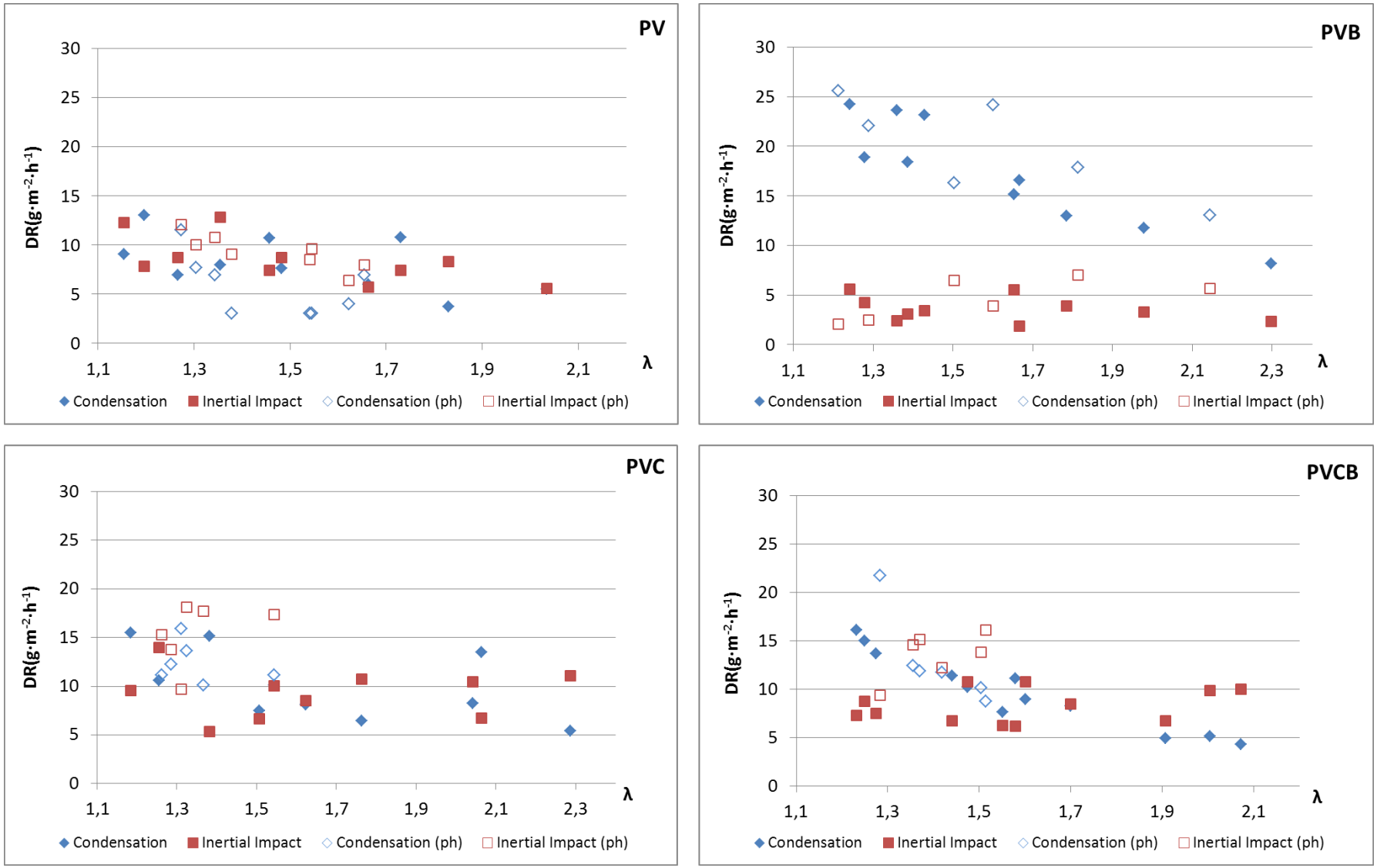

Fig. 4. Deposition rates (DR) by condensation and by inertial impact against excess air ratio (λ) to PV, PVB, PVC and PVCB.

343 Regarding tests without inlet air preheating, it can be verified that, for all fuels analyzed, deposition
344 by condensation clearly decreases as excess air ratio increases (for all fuels and within the range of λ
345 analyzed, there is a factor of about 3 between the highest and the lowest condensation deposition
346 rate values). The reason for this lies in the fact that a greater excess air ratio leads to a reduction of
347 combustion temperature, limiting the volatility of the main reactive ash elements that play a role in
348 deposition by condensation (mainly K, Cl and S) ([66], [67]).
349 In addition, the substantial values of deposition by condensation presented by PVB, especially at low
350 excess air ratios, are noteworthy. This is confirmed by the chemical analysis of the deposits:
351 • XRD analysis (see Table 5): PVB has a high percentage of KCl (37.4% on average in the four
352 samples analyzed, much higher than the other pellets) and K_2SO_4 (30.1% on average in the
353 four samples analyzed, only below PVCB).
354 • SEM-EDS analysis (see Fig.2 and Table 4): PVB presents the highest percentages of K and Cl,
355 and also of S.
356 However, there is no obvious correlation between these results and ash properties obtained in fuel
357 analysis (see Tables 1 and 2), as PVB presents lower concentrations of K and Cl than the other mixed
358 pellets, and lower concentration of S than PVCB. This fact corroborates that trying to predict the
359 performance of ash biomass based only on indices obtained from fuel analysis is not always accurate;
360 in fact, the usefulness of these indices has been questioned in other research works (e.g., [48], [56],
361 [68]-[70]).
362 Continuing with the results of tests without preheating, they also reveal that PV presents slightly
363 lower values of deposition rate by condensation than mixed pellets ($\leq$ 13 $g \cdot m^{-2} \cdot h^{-1}$ in all cases),
364 especially when excess air ratios are low. This fact is related to the different composition of these
365 deposits, which present low percentages of K_2SO_4 and, above all, of KCl detected by XRD (Table 5),
366 although this is partially compensated by the high percentage of $KHCO_3$ (25.3%, whereas in the rest
367 of fuels it is only detected in one PVB sample). The low concentration of KCl in the deposits can be
368 explained by the low concentration of Cl in this fuel (Tables 1 and 2). Concerning K_2SO_4, although PV

presents a high percentage of K and S (Tables 1 and 2), K has a greater affinity for P (it is found in very significant amounts in this fuel (Table 2)), what could facilitate the formation of K-phosphates before K-sulfates [24].

Concerning deposition by inertial impact, no common tendency has been found to apply to all fuels in tests without preheating. Whereas in PV its value clearly decreases when excess air ratio is higher, in mixed pellets it remains practically constant. These different tendencies among fuels may be caused by the fact that an increase in excess air ratio leads to two opposite effects that interact with different weights: on the one hand, increasing the air flow raises its speed in the bed, encouraging the entrainment of coarse fly ash; on the other hand, the adhesion of solid particles is discouraged, as sticky deposits in the ring (alkali metal sulfates and chlorides) become less substantial, owing to reduced vaporization and subsequent condensation.

To deepen the analysis of the behavior presented by each fuel, Table 6 shows total deposition rate, by condensation and by inertial impact, together with bottom ash proportion and sintering degree (fraction S2/3) as reflected by the experimental results presented in [41].

Table 6

Bottom ash proportion, sintering degree and deposition rates (total, by condensation and by inertial impact) mean values (range) of all tests without inlet air preheating.

	Bottom ash proportion [a]	**Sintering degree (fraction S2/3)**[a]	**DR**	**$DR_{Cond.}$**		**$DR_{Imp.}$**	
	%	**%**	**$g \cdot m^{-2} \cdot h^{-1}$**	**$g \cdot m^{-2} \cdot h^{-1}$**	**%**	**$g \cdot m^{-2} \cdot h^{-1}$**	**%**
PV	25.3 (18.1-31.3)	1.6 (0.3-3.1)	16.6 (11.0-21.3)	8.1 (3.7-13.0)	49.0 (31.0-62.5)	8.5 (5.5-12.8)	51.0 (37.5-69.0)
PVB	74.7 (72.8-77.7)	51.8 (26.7-62.2)	20.9 (10.5-29.9)	17.3 (8.2-24.3)	82.9 (73.4-90.8)	3.6 (1.9-5.6)	17.1 (9.2-26.6)
PVC	50.0 (48.3-50.7)	33.8 (23.5-40.7)	19.4 (14.2-25.0)	10.1 (5.4-15.5)	52.0 (32.9-74.1)	9.3 (5.3-14.0)	48.0 (25.4-67.1)
PVCB	59.5 (58.4-60.9)	40.1 (26.4-49.8)	19.2 (13.5-23.8)	9.7 (4.3-16.1)	54.0 (30.1-68.8)	8.3 (6.2-10.8)	46.0 (31.2-69.9)

[a] % with regard to total mass of ash introduced with the fuel.

Table 6 seems to indicate that, in mixed pellets, sintering prevents deposition by inertial impact by discouraging the entrainment of particles from the bed. As a result, PVB, which presents high sintering values, yields a much lower deposition rate by inertial impact values than PVC and PVCB.

The results of inlet air preheating tests (represented by unfilled markers in Fig. 4) can be used to corroborate this behavior of mixed pellets. Inlet air preheating increases air velocity in the bed, encouraging entrainment, but does not lead to a significant increase of combustion temperature [41]:

- Due to the fact that combustion temperature remains practically unchanged, ash vaporization and therefore deposition by condensation is not affected substantially by preheating for any of the mixed pellets.
- In contrast, it may be observed that air preheating largely increases deposition by inertial impact in PVC and PVCB, but much less in the case of PVB. In other words, an increase in air velocity causes a much bigger impact in particle entrainment and its subsequent deposition in fuels which are less susceptible to sintering.

The case of PV is somewhat different, because high entrainment (there is very little ash retention in the bed) does not directly translate, in tests without preheating, into a greater amount of deposits by inertial impact compared to that of other fuels, possibly owing to the lower quantity of sticky deposits. In fact, it seems that given that this fuel presents low concentrations of KCl and K_2SO_4, the sampling ring was saturated by deposits from inertial impact. As a result of this saturation, following an increase of excess air ratio and hence a decrease in sticky deposits due to condensation, the capacity of PV to retain deposits by inertial impact decreases (Fig. 4). It is worth analyzing the results of the tests with preheating for this fuel. First, a sharp decrease in deposition by condensation can be noticed compared with tests without preheating. This is due to the lower combustion temperatures reached in experiments with preheating [41], which discourages the evaporation of alkali metals from the bed, as expected in view of Table 5. The fact that KOH has greater affinity for SO_2/SO_3 and HCl than for CO_2 [24] explains at least partly the aforementioned non-appearance of K-carbonates in the preheated test. In addition, preheating of inlet air entails no significant increase of deposition by inertial impact, which reinforces the idea of saturation.

3.3.3. (K+Na)/(Cl+2S) molar ratios

To complete the comparative analysis of the various fuels, Table 7 shows (K+Na)/(Cl+2S) molar ratios, calculated from SEM results for deposit samples (Fig. 2), equation (3) and the initial analysis of the fuels (Tables 1 and 2).

Table 7
(K+Na)/(Cl+2S) molar ratios (mean values of tests with and without preheating).

	$(K+Na)_{Probe}$/(Cl+2S) deposits SEM	**$(K+Na)_{Cond.}$/(Cl+2S) deposits SEM**	**(K+Na)/(Cl+2S) Fuel analysis**
PV	2.13	1.71	3.16
PVB	1.26	1.21	4.08
PVC	1.11	1.01	6.02
PVCB	1.24	1.09	3.29

Regarding $(K+Na)_{Probe}$/(Cl+2S) molar ratio using total alkali metal concentration in deposits by SEM, it can be observed that all fuels present values higher than 1, i.e., there is an excess of alkali metals compared with Cl and S. The reasons for this are twofold:

- Part of K and Na have vaporized as hydroxides and condensed as carbonates (mainly $KHCO_3$, which was detected by XRD in PV and in one PVB sample, see Table 4).
- Ash entrainment of solid particles containing K and Na from the bed occurs.

If the second ratio is considered, $(K+Na)_{Cond.}$/(Cl+2S) -after discounting alkali metals compounds deposited in the sampling ring by inertial impact (following equation (3))- it can be noted that, in the case of PVCB and PVC, the value obtained is very close to 1 (practically all alkali metal have condensed as chlorides or sulfates), while in PVB and especially in PV it is higher, owing to the aforementioned presence of $KHCO_3$. The coherence of these ratios with XRD results corroborates that the hypotheses and assumptions on which equation (3) was based were sound.

Finally, it should be stressed that it is not possible to easily predict the values of these molar ratios (obtained by analyzing the deposits) nor to explain differences in the behavior of the various fuels on the basis of ratios calculated with fuels preliminary analysis (last column of Table 7), since there is no direct correspondence between them.

4. CONCLUSIONS

This study has presented the results of chemical analysis of deposits obtained in combustion tests carried out with four varieties of agropellet in a laboratory fixed-grate reactor. The analyses were carried by electron microscopy (SEM) with energy dispersive X-ray spectrometry (EDS) and X-ray diffractometry (XRD).

In order to take the results further, a simple methodology was developed that allows for deposits produced by condensation (including thermophoresis and turbulent diffusion) and by inertial impact of coarse fly ash entrained from the bed to be distinguished.

This methodology, alongside the results of chemical analysis and the data for deposition rates presented in a previous work [41], has yielded important results concerning the deposition phenomena affecting the four agropellets under study.

It was confirmed that an increase in excess air leads to a decrease in deposition by condensation, owing to a reduction in combustion temperatures, which limits the volatility of K, Cl and S. The lower deposition rates attested for PV could be related to its high P content.

However, concerning deposition by inertial impact, no common behavior has been found, probably because an increase in excess air ratio leads to two opposite effects. First, an increase in excess air ratio also increases the air flow, encouraging the entrainment of coarse fly ash. This effect becomes less acute as sintering increases; although sintering undermines the operation of the grate, it also discourages ash entrainment. Second, an increase in air excess ratio leads to a decrease of deposits by condensation, some of which take the shape of a sticky layer (mainly alkali metal sulfates and chlorides), and thus the adhesion of coarse fly ash entrained from the bed. In fact, at least concerning PV, it is argued that the adhesion of solid particles to sticky deposits can result in saturation.

The quantification of deposits produced by condensation and by inertial impact, although achieved through a series of simplifications and assumptions, provides useful information which, it is hoped, will contribute to finding solutions to the problem posed by high deposition rates in the combustion

of agricultural residual biomass, leading to both better fuel blends and boiler design and operational parameters, increasing the market penetration of this important kind of biomass.

As noted, fly ash deposition and bottom ash sintering are related; sintering and the relationship between both phenomena will be addressed in depth from bottom ash chemical characterization, as part of complementary further research studies.

5. ACKNOWLEDGEMENTS

The authors greatly acknowledge the Spanish Ministry of Science, Innovation and Universities for funding the project "MHWPellet: Mixed pellets based on agricultural crops residues (herbaceous and woody) for their use in the residential sector: optimization of their composition and conversion parameters" (ref. ENE2015-68809-R (MIMECO/FEDER, UE)).

Authors also would like to acknowledge the use of *Servicio General de Apoyo a la Investigación-SAI, Universidad de Zaragoza*.

6. REFERENCES

[1] Scarlat N, Dallemand JF, Monforti-Ferrario F, Banja M. Renewable energy policy framework and bioenergy contribution in the European Union – An overview from National Renewable Energy Action Plans and Progress Reports. Renewable and Sustainable Energy Reviews 2015; 51: 969-985.

[2] Scarlat N, Dallemand JF, Monforti-Ferrario F, Nita V. The role of biomass and bioenergy in a future bioeconomy: Policies and facts. Environmental Development 2015; 15: 3-34.

[3] Bozell JJ, Black SK, Myers M, Cahill D, Miler WP, Park S. Solvent fractionation fo renewable woody feedstocks: Organoslv generation of biorefinery process streams for the production of biobased chemicals. Biomass Bioenergy 2011; 35(10): 4197-208

[4] Food and Agricultural Organization of the United Nations – FAOSTAT - http://www.fao.org/faostat/ , accessed in May 2019

[5] Carvalho L, Wopienka E, Pointner C, Lundgren J, Verma VK, Haslinger W, Schamidl C. Performance of a pellet boiler fired with agricultural fuels. Applied Energy 2013; 104: 286-296.

[6] Sippula O, Hytönen K, Tissari J, Raunemaa T, Jokiniemi J. Effect of Wood Fuel on the Emissions from a Top-Feed Pellet Stove. Energy & Fuels 2007; 21 (2): 1151-1160.

[7] Houshfar E, Lovas T, Skreiberg O. Experimental Investigation on NOX Reduction by Primary Measures in Biomass Combustion: Straw, Peat, Sewage Sludge, Forest Residues and Wood Pellets. Energies 2012; 5 (2): 270-290.

[8] Díaz-Ramírez M, Sebastian F, Royo J, Rezeau A. Influencing factors on NOX emission level during grate conversion of three pelletized energy crops. Applied Energy 2014; 115 (0): 360-373.

[9] Wang L, Skjevrak G, Hustad JE, Gronli M, Skreiberg O. Effects of Additives on Barley Straw and Husk Ashes Sintering Characteristics. Energy Procedia 2012;20:30-39

[10] Glarbor P, Marshall P. Mechanism and modeling of the formation of gaseous alkali sulfates Combustion and Flame 2005;141:22–39

[11] Garba MU, Ingham DB, Ma L, Porter RTJ, Pourkashnian M, Tan HZ, Williams A. Prediction of Potassium Chloride Sulfation and Its Effect on Deposition in Biomass-Fired Boilers EnergyFuels 2012; 26: 6501−08

[12] Niu Y, Tan H, Hui S. Ash-related issues during biomass: Alkali-induced slagging, silicate melt-induced slagging (ash fusion), agglomeration, corrosion, ash utilization, and related countermeasures. Progress in Energy and Combustion Science 2016; 52: 1-61

[13] Capablo J. Formation of alkali salt deposits in biomass combustion. Fuel Processing Technology 2016; 153: 58–73

[14] Johansson L.S., Leckner B., Gustavsson L. Cooper D., Tullin C., Potter A. Emission characteristics of modern and old-type residential boilers fired with wood logs and wood pellets. Atmospheric Environment 2004; 38 (25), 4183-4195.

514 [15] Obernberger I., Biedermann F., widmann W., Riedl R. Concentrations of inorganic elements in
515 biomass fuels and recovery in the different ash fractions. Biomass and Bioenergy 1997; 12 (3),
516 211-224.
517 [16] Wierzbicka A., Lillieblad L., Pagels J., Strand M., Gudmundsson A., Gharibi A., Swietlicki E.,
518 Sanati M., Bohgard M. Particle emissions from district heating units operating on three
519 commonly used biofuels. Atmospheric Environment 2005; 39 (1), 139-150.
520 [17] Wiinikka H., Gebart R., Boman C., Boström D., Öhman M. Influence of fuel ash composition on
521 high temperature aerosol formation in fixed bed combustion of woody biomass pellets. Fuel
522 2007; 86 (1-2), 181-193.
523 [18] Wiinikka H., Gebart R. Experimental investigations of the influence from different operating
524 conditions on the particle emissions from a small-scale pellets combustor. Biomass and
525 Bioenergy 2004; 27 (6), 645-652.
526 [19] Brunner T., Obernberger I., Scharler R. Primary measures for low-emission residential wood
527 combustion-Comparison of old with optimised modern systems. Proceedings of 17th European
528 Biomass Conference and Exhibition, Hamburg, Germany, 2009, 1319-1328.
529 [20] Obernberger I., Brunner T., Bärnthaler G. Chemical properties of solid biofuels--significance
530 and impact. Biomass and Bioenergy 2006; 30 (11): 973-982.
531 [21] Díaz-Ramírez M., Boman C., Sebastian F., Royo, J., Xiong S., Boström D. Ash Characterization
532 and Transformation Behavior of the Fixed-Bed Combustion of Novel Crops: Poplar, Brassica,
533 and Cassava Fuels. Energy & Fuels 2012; 26 (6): 3218-3229.
534 [22] Díaz-Ramírez, M., Sebastian F., Royo J., Rezeau A. Combustion requirements for conversion of
535 ash-rich novel energy crops in a 250 kWth multifuel grate fired system. Energy 2012; 46 (1):
536 636-643.
537 [23] Díaz-Ramírez M., Frandsen F.J., Glarborg P., Sebastian F., Royo J. Partitioning of K, Cl, S and P
538 during combustion of poplar and brassica energy crops. Fuel 2014; 134 (0): 209-219.

539 [24] Boström D, Skoglund N, Grimm A, Boman C, Ohman M, Brostrom M, Backman R. Ash
540 transformation chemistry during combustion of biomass. Energy & Fuels 2012; 26: 85–93.
541 [25] Becidan M, Houshfar E, Khalil RA, Skreiberg Ø, Løvås T, Sørum L. Optimal Mixtures to Reduce
542 the Formation of Corrosive Compounds during Straw Combustion: A Thermodynamic Analysis.
543 Energy & Fuels 2011; 25: 3223-3234
544 [26] Khor A, Ryu C, Yang Y-b, Sharifi VN, Swithenbank J. Straw combustion in a fixed bed
545 combustor. Fuel 2007; 86: 152-160
546 [27] Magdziarz A, Dalai AK, Koziński JA. Chemical composition, character and reactivity of
547 renewable fuel ashes. Fuel 2016; 176: 135-145
548 [28] Fernández-Llorente MJ, Escalada-Cuadrado R, Murillo-Laplaza JM, Carrasco-García JE.
549 Combustion in bubbling fluidised bed with bed material of limestone to reduce the biomass
550 ash agglomeration and sintering. Fuel 2006; 85 (14-15): 2081-2092.
551 [29] Knudsen JN, Jensen PA, Dam-Johansen K. Transformation and release to the gas phase of Cl, K,
552 and S during combustion of annual biomass. Energy & Fuels 2004; 18 (5): 1385-1399.
553 [30] van Lith SC, Alonso-Ramírez V, Jens PA, Frandsen FJ, Glarborg P. Release to the gas phase of
554 inorganic elements during wood combustion. Part 1: Development and evaluation of
555 quantification methods. Energy & Fuels 2006; 20 (3): 964-978.
556 [31] Theis M, Skrifvars BJ, Hupa M, Tran H. Fouling tendency of ash resulting from burning mixtures
557 of biofuels. Part 1: deposition rates. Fuel, 2006; 85: 1125–1130
558 [32] Li G, Li S, Xu X, Huang Q, Yao Q. Dynamic behavior of biomass ash deposition in a 25 kW one-
559 dimensional down-fired combustor. Energy & Fuels, 2013; 28: 219-227
560 [33] Ryu C, Yang YB, Khor A, Yates NE, Sarifi VN, Swithenbank J. Effect of fuel properties on biomass
561 combustion: Part I. Experiments – fuel type, equivalence ratio and particle size. Fuel, 2006; 85
562 (7-8): 1039-1046

563 [34] Houshfar E, Khalil RA, Lovas T, Skriberg O. Enhanced NOx Reduction by Combined Staged Air
564 and Flue Gas Recirculation in Biomass Grate Combustion. Energy & Fuels, 2012. 26(5): 3003-
565 3011.
566 [35] Zhou H, Jensen AD, Glarborg P, Kavaliauskas A. Formation and reduction of nitric oxide in
567 fixed-bed combustion of straw. Fuel, 2006; 85 (5-6): 705-716
568 [36] Andzi-Barhe T, Rogaume T, Richard F, Torero JL. Numerical characterisation of the mechanisms
569 of NOx formation during MSW incineration.MCS6. 2009. Ajaccio (France).
570 [37] Brunner T, Biedermann F, Kanzian W, Evic N, Obernberger I. Advanced Biomass Fuel
571 Characterization Based on Tests with a Specially Designed Lab-Scale Reactor. Energy & Fuels,
572 2013; 27 (10): 5691-5698.
573 [38] Wiinikka H and Gebart R. Experimental investigations of the influence from different operating
574 conditions on the particle emissions from a small-scale pellets combustor. Biomass and
575 Bioenergy, 2004. 27(6): p. 645-652.
576 [39] Zhou H, Jensen AD, Glarborg P, Jensen PA, Kavaliauskas A. Numerical modeling of straw
577 combustion in a fixed bed. Fuel, 2005; 84: 389-403.
578 [40] Wiinikka H and Gebart R. Critical Parameters for Particle Emissions in Small-Scale Fixed-Bed
579 Combustion of Wood Pellets. Energy & Fuels, 2004. 18(4): p. 897-907.
580 [41] Royo J, Canalís P, Quintana D, Díaz-Ramírez M, Sin A, Rezeau A. Experimental study on the ash
581 behaviour in combustion of pelletized residual agricultural biomass. Fuel, 2019; 239: 991-1000.
582 [42] Vassilev, S. V., and Vassileva, C. G. Methods for characterization of composition of fly ashes
583 from coal-fired power stations: A critical overview. Energy & Fuels, 2005; 19:1084-1098.
584 [43] Deng L., Jin, X., Long, J., Che, D. Ash deposition behaviors during combustion of raw and water
585 washed biomass fuels. Journal of the Energy Institute (2018)
586 https://doi.org/10.1016/j.joei.2018.07.009

587 [44] Fernández, M. J., Mediavilla, I., Barro, R., Borjabad, E. Ramos, R. Carrasco, J. E. Sintering
588 reduction of herbaceous biomass when blended with woody biomass: predictive and
589 combustion tests. Fuel (2019) 239:1115–1124
590 [45] Imran M, Khan A. Characterization of Agricultural Waste Sugarcane Bagasse Ash at 11000C
591 with various hours. Materials Today: Proceedings 2018; 5: 3346–3352
592 [46] Liu Y, He Y, Wang Z, Xia J, Wan K, Whiddon R, Cen K. Characteristics of alkali species release
593 from a burning coal/biomass blend. Applied Energy 2018;215:523-531
594 [47] Fernández-Llorente J, Díaz-Arocas P., Gutiérrez Nebot L, Carrasco-García JE. The effect of the
595 addition of chemical materials on the sintering of biomass ash. Fuel 2008; 87:2651–58
596 [48] Wang L, Skreiberg Ø, Becidan M. Investigation of additives for preventing ash fouling and
597 sintering during barley straw combustion. Applied Thermal Engineering 2014; 70:1262-69
598 [49] Nunes LJR, Matias JCO, Catalao JPS. Biomass combustion systems: A review on the physical and
599 chemical properties of the ashes. Renewable and Sustainable Energy Reviews, 2016; 53:235-
600 242.
601 [50] Porteiro J., Patiño D., Collazo J., Granada E., Moran J., Miguez J.L. Experimental analysis of the
602 ignition front propagation of several biomass fuels in a fixed-bed combustor. Fuel, 2010; 89:
603 26-35
604 [51] Díaz-Ramirez M., Maraver D., Rezeau A. Royo J., Sala S., Sebastian F., Sin A.Estimation of the
605 deposition on trigeneration system components fueled by ash rich biomass. Proceedings of
606 20th European Biomass Conference and Exhibition, Milan, Italy (2012) 774-780
607 [52] Jensen PA, Stenholm M, Hald P. Deposition investigation in straw-fired boilers. Energy Fuels
608 1997;11:1048-55
609 [53] Kaufmann H, Nussbaumer T, Baxter L, Yang N. Deposit formation on a single cylinder during
610 combustion of herbaceous biomass. Fuel, 2000; 79: 141–51
611 [54] Weber R, Poyraz Y, Beckmann M, Brinker S. Combustion of biomass in jet flames. Proceedings
612 of the Combustion Institute, 2015; 35: 2749–2758

613 [55] Lokare SS, Dunaway JD, Moulton D, Rogers D, Tree DR, Baxter LL. Investigation of ash
614 deposition rates for a suite of biomass fuels and fuel blends. Energy and Fuels, 2006; 20(3):
615 1008–14.
616 [56] Regueiro A, Patiño D, Granda E, Porteiro J. Experimental study on the fouling behaviour of an
617 underfeed fixed-bed biomass combustor. Applied Thermal Engineering, 2017; 112: 523–533
618 [57] Zeng T., Pollex T., Weller N., Lenz V., Nelles M. Blended biomass pellets as fuel for small scale
619 combustion appliances: Effect of blending on slag formation in the bottom ash and pre-
620 evaluation options. Fuel 2018; 212: 108-116
621 [58] Öhmana M., Bomana C., Hedmanb H., Nordina A., Boström D. Slagging tendencies of wood
622 pellet ash during combustion in residential pellet burners. Biomass and Bioenergy 2004; 27:
623 585–596
624 [59] Zevenhoven M, Yrjas P, Skrifvars BJ, Hupa M. Characterization of ash-forming matter in various
625 solid fuels by selective leaching and its implications for fluidized-bed combustion. Energy and
626 Fuels 2012; 26:6366–86.
627 [60] Niu YQ, Tan HZ, Ma L, Pourkashanian M, Liu ZN, Liu Y, Wang X, Liu H, Xu T. Slagging
628 characteristics on the superheaters of a 12 MW biomass-fired boiler. Energy and Fuels 2010;
629 24: 5222-7
630 [61] Niu YQ, Tan HZ, Wang XB, Liu ZN, Liu Y, Xu TM. Study on deposits on the surface, upstream,
631 and downstream of bag filters in a 12 MW biomass-fired boiler. Energy and Fuels 2010;
632 24:2127–32.
633 [62] Mu L, Zhao L, Liu L, Yin H. Elemental distribution and mineralogical composition of ash deposits
634 in a large-scale wastewater incineration plant: a case study. Industrial and Engineering
635 Chemical Research 2012; 51:8684–94.
636 [63] Wei XL, Schnell U, Hein KRG. Behaviour of gaseous chlorine and alkali metals during biomass
637 thermal utilisation. Fuel 2005; 84:841–8.

638 [64] Díaz-Ramírez MC. Grate-Fired Energy Crop Conversion: Experiences with Brassica Carinata and
639 Populus sp. Ed. Springer Theses 2015; ISBN 978-3-319-20758-2
640 [65] Vassilev S.V., Baxter B., Vassileva C.G. An overview of the behaviour of biomass during
641 combustion: Part I. Phase-mineral transformations of organic and inorganic matter. Fuel, 2013;
642 112:391–449
643 [66] Theis M., Skrifvars B.-J., Zevenhoven M., Hupa M., Tran H. Fouling tendency of ash resulting
644 from burning mixtures of biofuels. Part 2: deposit chemistry. Fuel, 2006; 85: 1992–2001.
645 [67] Thy P, Jenkins BM, Grundvig S, Shiraki R, Lesher CE. High temperature elemental losses and
646 mineralogical changes in common biomass ashes. Fuel, 2006; 85:783–95.
647 [68] Vassilev S. V., Baxter D., Vassileva C. G. An overview of the behaviour of biomass during
648 combustion: Part II. Ash fusion and ash formation mechanisms of biomass types. Fuel, 2014;
649 117: 152–183
650 [69] García-Maraver A., Zamorano M., Fernandes U., Rabaçal M,. Costa M. Relationship between
651 fuel quality and gaseous and particulate matter emissions in a domestic pellet-fired boiler.
652 Fuel, 2014; 119: 141-152
653 [70] Xiao R., Chen X., Wang F., Yu G. The physicochemical properties of different biomass ashes at
654 different ashing temperature. Renewable Energy, 2011; 36: 244-249